Journal of Computer-Aided Molecular Design, 11 (1997) 345–356.

J-CAMD 401

Electron affinities of *p*-benzoquinone, *p*-benzoquinone imine and *p*-benzoquinone diimine, and spin densities of their *p*-benzosemiquinones computed by several quantum chemical models

Yitbarek H. Mariam* and Lek Chantranupong

Department of Chemistry and Center for Theoretical Studies of Physical Systems, Clark Atlanta University, Atlanta, GA 30314, U.S.A.

Received 9 August 1996
Accepted 12 March 1997

Keywords: *p*-Benzoquinone; *p*-Benzoquinone imine; *p*-Benzosemiquinone radicals; 5-Iminodaunomycin; Anthracyclines; Adiabatic electron affinities; Spin densities; Density functional method (DFT); Hybrid Hartree–Fock/density functional; B3LYP

Summary

Restricted and unrestricted (U) Hartree–Fock (HF), second-order Møller–Plesset perturbation (MP2), density functional (DF), hybrid HF/DF and semiempirical (half-electron (HE) method) models have been used to calculate adiabatic electron affinities (EA_{ad} values) of *p*-benzoquinone (**I**), *p*-benzoquinone imine (**VI**) and *p*-benzoquinone diimine (**XI**), as well as expectation values ($\langle S^2 \rangle$) and spin density distributions in the radical anions of **I**, **VI** and **XI**. The AM1/AM1-HE and ab initio calculated structures are found to be in accord with each other. The ROHF/6-31G(d) method gave the poorest EA_{ad} result. The UHF and UMP2 wave functions were found to be substantially spin contaminated (for the radicals) and the accuracies of the EA_{ad} values calculated were also poor. The use of molecular energies obtained after spin annihilation did not lead to significant improvement of the UHF and UMP2 results. In contrast to the ROHF, UHF and UMP2 results, the DF(USVWN, UBVWN, UBLYP) and hybrid HF/DF(UB3LYP) methods, as well as the AM1-HE, gave much better results. The calculated EA_{ad} values decreased, as predicted by most of the models, in the order EA_{ad}(**I**) > EA_{ad}(**VI**) > EA_{ad}(**XI**). The differences in the EAs, EA_{ad}(**I**) – EA_{ad}(**VI**) and EA_{ad}(**I**) – EA_{ad}(**XI**), were consistently predicted to be about 8–9 and 17–18 kcal/mol, respectively, by the DF, B3LYP and AM1-HE models. The performance of the PM3 and SAM1 models was not as good as the AM1 model. Of all the methods tested, the B3LYP/6-311G(d,p) model is concluded to give the most accurate quantitative trend (**I**(42.6) > **VI**(33.1) > **XI**(23.7)) in EA_{ad}. The predicted trend in EA can satisfactorily be rationalized by the calculated LUMO orbital energies, atomic charges and spin density distributions. Analysis of the spin density data predicts that phenoxyl- and anilino-type radical anions predominate in the *p*-benzosemiquinones of **I** and **XI**, respectively, while both phenoxyl- and anilino-type radicals contribute to the structure of the *p*-benzosemiquinone of **VI**, with the anilino-type predominating.

Introduction

Despite the tremendous amount of experimental work on the anthracyclines, there are still some structure–activity relationships that remain unresolved [1], particularly with regard to the effects of modification of the hydroxyquinone functionality in daunomycin (DN) and adriamycin (AD) (**1a** and **1b**, Scheme 1). The focus on the hydroquinone functionality stems from considerable evidence that points to this functionality being responsible for both antitumor activity and cardiac toxicity of the anthracyclines [2]. In the case of 5-iminodaunomycin (5IDN) (**2**, Scheme 1), in which one of the carbonyl functionalities of the biochemically active site in DN has been altered to an imine, little or no cardiac toxicity was shown, although the drug appeared to show antitumor activity in several commonly used marine tumor models and human tumor xenographs [2]. The lower cardiotoxicity of 5IDN has been attributed to its diminished capacity for catalytically producing reactive oxygen species [3], and, because of this property, 5IDN has been described as a 'redox-incapacitated' anthracycline [4]. These conclusions stemmed from the electrochemical results of Lown et al. [3a,b], which indicated that an aqueous solution of 5IDN was

*To whom correspondence should be addressed.

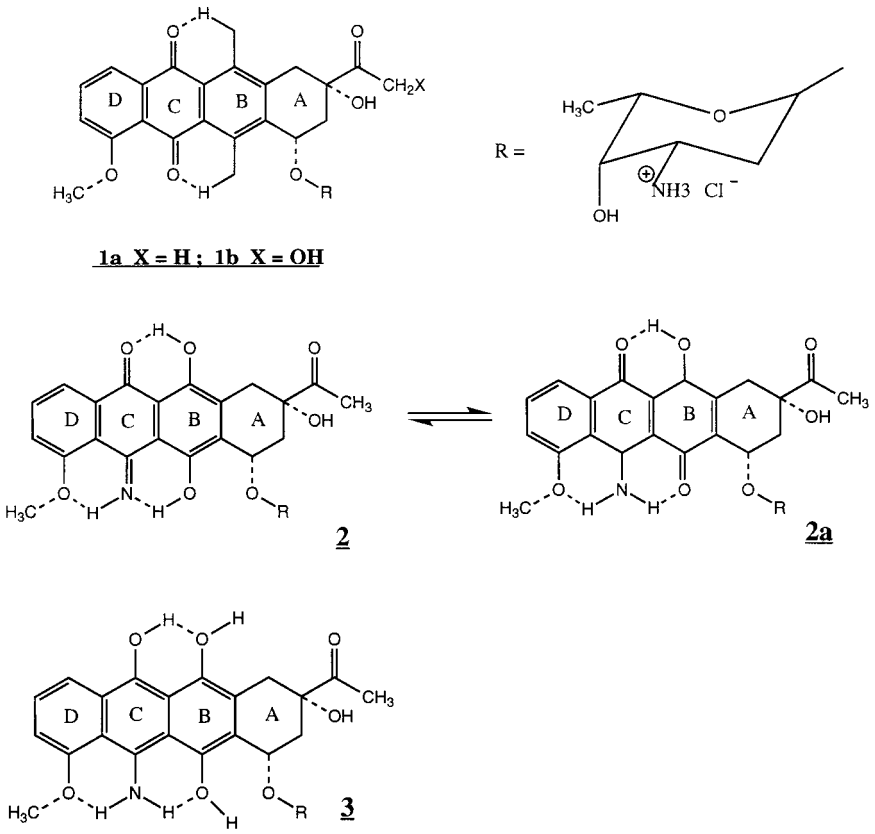

Scheme 1. Structural representations of daunomycin (**1a**), adriamycin (**1b**), 5-iminodaunomycin (**2**) and 5,11-dihydro-5-iminodaunomycin (**3**).

more difficult to reduce than DN and that the reoxidation of the reduced 5IDN (5,11-dihydro-5-iminodaunomycin (**3**, Scheme 1)) in aqueous solution was much more difficult than the reoxidation of the reduced DN.

The redox chemistry of the anthracyclines involves reductive activation and autoxidation, termed 'redox cycling', the specific reactions being electron and proton attachments (for reductive activation), and detachments (for autoxidation) [5]. The autoxidation process is presumed to be accompanied by the reduction of molecular oxygen to reactive oxygen species (superoxide anion, hydroperoxide, hydrogen peroxide, etc.) which may ultimately be the actual species responsible for toxicity in general, and for cardiotoxicity in particular, of the anthracyclines [6].

In an effort to get more insight into the above redox chemistry of the anthracyclines, we have recently investigated, by semiempirical methods, the trends in the reactivity of *p*-benzoquinone (**I**), *p*-benzoquinone imine (**VI**) and *p*-benzoquinone diimine (**XI**) as the simplest model systems for the pharmacophorically important quinone site of the anthracyclines [7]. Some of the conclusions of that study were: (a) trends in redox capacity and electron affinity (EA) can be predicted by the computationally expedient AM1 and SAM1 methods; and (b) the 'redox incapacitation' of 5IDN may be explained by two factors, namely (i) diminished electron affinity, particularly in the first electron attachment step of the reductive process, leading to diminished reducibility and (ii) greater deprotonation energy of the semiquinone and hydroquinone forms, leading to diminished autoxidizability; (iii) the combined effect of these factors should lead to a reduced efficiency in redox cycling. In the light of the incompletely delineated micromechanisms of the modes of action of the anthracyclines, the above findings can be very significant and further work by more accurate methods is necessary to establish these findings on firmer ground. Besides the above practical significance of the biochemical/biomedical problem, a brief overview of some of the electron affinity data (Y.H. Mariam, unpublished results) obtained from the initial studies [7; Y.H. Mariam, unpublished results] and the methods used for these studies can illustrate the need for further systematic study.

From the outset, the calculation of EAs for a molecule M is generally problematic for several reasons [8]. These include: the need to accurately describe the geometries of M and the corresponding anion M^-; the need to accurately account for the difference in electron correlation energies in M and M^-; and the need to ascertain that appropriate basis sets have been employed. In those cases where spin contamination is substantial, the standard ab initio and semiempirical unrestricted Hartree–Fock (UHF) formalisms are not adequate (since the wave functions are not eigenfunctions of the spin operator $\hat{S}^2$) and methods that remedy the spin contamination problem are needed.

Additionally, although semiempirical molecular orbital (MO) methods are computationally expedient for the investigations of relatively large molecules, the approximations used in these methods may not warrant the accuracy of molecular parameters, such as electron affinity, that are obtainable from such methods. This is particularly important in those cases where the systems to be investigated involve neutral and ionic radicals, because the representation of ions and free radicals in the training sets used for parametrization was probably sparse.

Because the AM1 UHF formalism gave substantial spin contamination for the radical anions of **I**, **VI** and **XI**, adiabatic EAs (48.7, 40.7 and 32.9 kcal/mol for **I**, **VI** and **XI**, respectively) were determined using the AM1 half-electron (AM1-HE) method [9]. In contrast to the AM1-HE EA of **I**, Dewar and Rzepa [10] had reported an adiabatic EA of 43.4 kcal/mol from MNDO-HE calculations. Since the experimental gas-phase electron attachment free energy of **I** (at 300 K) has been reported to be about 43 kcal/mol [11,12], the AM1-HE method clearly overestimates the EA of **I** by about 6 kcal/mol. The overestimation of the EA_{ad} of **I** by the AM1-HE method is also unlike the results obtainable from ab initio HF methods which generally underestimate EAs. That the ab initio HF methods underestimate EAs is particularly true for the systems of interest here (as will be shown later). For example, the adiabatic EAs of **I** as determined by UHF/3-21G(d) and UHF/6-31G(d)//3-21G(d) were 22.9 and 16.6 kcal/mol, respectively. Part of the reason for the underestimation of the HF EAs may be because the HF model does not include correlation effects at all. Nevertheless, even unrestricted second-order Møller–Plesset (MP2) calculations gave results that were not significantly better than the UHF results. The UMP2/6-31G(d)//UHF/3-21G(d) adiabatic EA of **I** was, for example, calculated to be only 21.5 kcal/mol. Since AM1 is parametrized to experimental

TABLE 1
COMPARISON OF BOND LENGTHS[a] AND BOND ANGLES[a] OF **I**, **VI** AND **XI** CALCULATED BY AM1, MP2, SVWN AND B3LYP METHODS

	I				**VI**				**XI**			
	AM1	MP2[b]	SVWN[c]	B3LYP[b]	AM1	MP2[b]	SVWN[c]	B3LYP[b]	AM1	MP2[b]	SVWN[c]	B3LYP[b]
Bond length (Å)												
C1=O	1.236	1.238	1.221	1.225	1.237	1.239	1.223	1.227				
C4=O	1.236	1.238	1.221	1.225								
C2=C3	1.338	1.349	1.338	1.343	1.339	1.350	1.340	1.345	1.339	1.351	1.341	1.345
C5=C6	1.338	1.349	1.338	1.343	1.339	1.350	1.340	1.345	1.339	1.351	1.341	1.345
C1-C2	1.479	1.481	1.468	1.486	1.477	1.476	1.466	1.481	1.479	1.467	1.452	1.472
C3-C4	1.479	1.481	1.468	1.486	1.481	1.466	1.454	1.472	1.478	1.467	1.452	1.471
C4-C5	1.479	1.481	1.468	1.486	1.482	1.469	1.453	1.475	1.479	1.465	1.452	1.472
C1-C6	1.479	1.481	1.468	1.486	1.474	1.479	1.462		1.478	1.465	1.452	
C4=N					1.290	1.299	1.286	1.289	1.291	1.300	1.287	1.291
N-H					0.999	1.030	1.034	1.027	0.999	1.030	1.033	1.027
C1=N									1.291	1.300	1.287	1.287
N-H									0.999	1.030	1.033	1.027
C2-H	1.103	1.087	1.095	1.086	1.102	1.087	1.094	1.086	1.104	1.087	1.094	1.088
C3-H	1.103	1.087	1.095	1.086	1.104	1.087	1.097	1.086	1.103	1.089	1.096	1.068
C5-H	1.103	1.087	1.095	1.086	1.104	1.090	1.094	1.089	1.104	1.087	1.094	1.088
C6-H	1.103	1.087	1.095	1.086	1.103	1.087	1.094	1.086	1.103	1.089	1.096	1.086
Bond angle (°)												
C2-C1-O7	122.0	121.2	121.3	121.3	122.1	121.1	121.3	122.0				
C3-C4-O8	122.0	121.2	121.3	121.4								
C3-C4-N8					125.4	124.9	124.5	118.0	125.7	125.4	125.1	118.0
C2-C1-C6	116.1	117.6	117.5	117.3	115.5	117.1	116.8	116.7	114.4	117.2	117.0	125.4
C3-C4-C5	116.1	117.6	117.5	117.3	115.0	117.8	117.6	117.2	114.3	117.2	117.0	116.6
C1-C2-C3	122.0	121.2	121.3	121.4	122.0	121.4	121.4	121.5	122.3	121.5	121.5	116.6
C1-C6-C5	122.0	121.2	121.3	121.4	122.6	121.2	121.4	121.5	123.2	121.3	121.5	121.6
C2-C3-C4	122.0	121.2	121.3	121.4	122.6	121.2	121.3	121.7	123.2	121.3	121.5	121.8
C6-C5-C4	122.0	121.2	121.3	121.4	122.2	121.4	121.4	121.5	122.2	121.5	121.5	121.8
C1-C2-H	115.7	116.3	115.5	115.9	115.8	116.4	115.7	116.1	116.6	116.2	115.6	121.6
C2-C3-H	122.3	122.6	123.2		120.7	121.0	121.5		120.3	120.8	121.2	117.4
C4-N8-H					115.6	110.0	110.0	110.3	115.3	109.6	109.8	110.2
C1-N7-H									115.3	109.8	109.8	110.2

[a] Atom numbering as shown in Scheme 3.
[b] 6-31G(d) basis set.
[c] 6-311G(d,p) basis set.

data, it presumably includes some correlation effects, thus giving somewhat better results. But, what level of credence can be given to the trend observed by the AM1 method cannot be ascertained in the absence of additional evidence.

Similarly, preliminary results from density functional (DF) calculations (using the local spin density approximation and the Vosko, Wilk and Nusair [13] correlation functional (LSDA/VWN) and UHF/3-21G(d) geometry) gave adiabatic EAs of 54.9, 44.3 and 35.3 kcal/mol, respectively, for **I**, **VI** and **XI**. The LSDA/VWN model which includes dynamic correlation, thus, overestimates the EA of **I** (and probably that of **VI** and **XI**) by about 12 kcal/mol. This overestimation is unlike the results of Ziegler and Gutsev [8], who showed that the local density approximation (LDA) underestimates adiabatic electron affinities, on average, by 0.4 eV. The systems they investigated were, however, substantially smaller than, and without as much conjugation, if any, as the systems of interest here. Use of the Barth–Hedin exchange-correlation model potential (LSDA/VBH//UHF/3-21G(d) [14]) also gave similar values of adiabatic EAs (57.1, 48.3 and 37.8 kcal for **I**, **VI** and **XI**, respectively). Clearly, such variations in computed results by various models cannot be resolved without additional evidence from computational or experimental results, or both.

In the light of the previously mentioned biochemical/biomedical interest in *p*-benzoquinone (which is ubiquitous in nature) and *p*-benzoquinone imine, and the above quantum chemical considerations/observations, it was deemed necessary to compute the electron affinities of **I**, **VI** and **XI** by a variety of methods: ab initio molecular orbital, density functional (DF) and hybrid Hartree–Fock/density functional (HF/DF) quantum chemical models. Within each model, several formalisms and/or basis sets have been explored and the results will be compared with those from semiempirical models as well as with experiment where available. Conventional analysis of the calculated structural data will be made both to see how well the AM1 geometry can compare with ab initio results, and to glean information on salient and/or distinct structural differences between the model systems upon electron attachment. Analysis of the spin density data will also be made to seek any differences in the radical anions. Finally, an attempt to establish a quantitative trend in the adiabatic EAs of **I**, **VI** and **XI**, and also to rationalize the calculated trend in EA, will be made.

Computational details

Adiabatic electron affinities (EA_{ad}'s) were calculated using the definition for EA_{ad} [8]:

$$EA_{ad} = E_0(Q) - E_0(Q^{\bullet -}) \quad (1)$$

where $E_0(Q)$ is the energy of the neutral systems **I**, **VI** and **XI**, and $E_0(Q^{\bullet -})$ is the energy of the corresponding radical anions, $Q^{\bullet -}$ of **I**, **VI** and **XI**, when both are in their electronic and vibrational ground states. Calculations on Q and $Q^{\bullet -}$ were done using, respectively, restricted and unrestricted formalisms. UHF, UMP2, HF, MP2, spin-restricted and spin-unrestricted DF, and hybrid

TABLE 2
COMPARISON OF BOND ANGLES IN THE $Q^{\bullet -}$ FORMS OF **I**, **VI** AND **XI** CALCULATED BY THE B3LYP/6-31G(d) MODELS[a,b], AND CALCULATED CHANGES IN B3LYP/6-31G(d) BOND LENGTHS UPON ELECTRON ATTACHMENT[a,b,c]

Angle	Bond angles (°)			Bond	Changes in bond length[a] (Å)		
	I	**VI**	**XI**		**I**	**VI**	**XI**
C2-C1-O7	122.7	123.0		C1=O	0.042	0.039	
C3-C4-O8	122.7			C4=O	0.042		
C3-C4-N8		125.8	119.8	C2=C3	0.029	0.031	0.029
C2-C1-N7			126.1	C5=C6	0.029	0.027	0.029
C2-C1-C6	114.6	113.8	114.1	C1-C2	–0.033	–0.033	–0.026
C3-C4-C5	114.6	114.7	114.1	C3-C4	–0.033	–0.031	–0.028
C1-C2-C3	122.7	122.8	123.1	C4-C5	–0.033	–0.028	–0.026
C1-C6-C5	122.7	123.0	122.9	C1-C6	–0.033	–0.027	–0.028
C2-C3-C4	122.7	122.8	122.9	C1-N7			0.047
C6-C5-C4	122.7	122.7	123.1	C4=N		0.049	0.047
C1-C2-H	116.2	116.5	117.4	N7-H		0.003	0.003
C4-N8-H		107.3	107.3	N8-H			0.003
C1-N7-H		107.3		C2-H	0.004	0.004	0.005
				C3-H	0.004	0.004	0.004
				C5-H	0.004	0.004	0.005
				C6-H	0.004	0.004	0.004

[a] Atomic numbering as in Scheme 3.
[b] Bond angles and calculated changes in bond lengths at the B3LYP/6-311G(d,p) level are not included here, but the results were essentially unchanged from that at the B3LYP/6-31G(d) level.
[c] Positive and negative values represent the increase and decrease in bond length of a given bond upon electron attachment.

TABLE 3
COMPARISON OF SELECTED BOND LENGTHS OF *p*-BENZOSEMIQUINONE RADICALS OF **I**, **VI** AND **XI** WITH CORRESPONDING BOND LENGTHS IN THE PHENOXYL RADICAL, PHENOL AND ANILINE

Calculated (B3LYP/6-31G(d))					Experimental[a]		
Bond	**I**[b]	**VI**[b]	**XI**[b]	Phenoxyl radical[c]	Bond	Phenol	Aniline
C1-O	1.267	1.271		1.268	C-O	1.364	
C2-C3	1.372	1.376	1.374	1.386	C-C(av)	1.397	1.392
C1-C2	1.453	1.448	1.446	1.467			
C-N		1.338	1.338		C-N		1.431

[a] Reference 39.
[b] This work.
[c] Reference 30.

HF/DF calculations were performed using the GAUSSIAN94/DF suite of programs [15] unless otherwise specified. Full geometry optimizations were carried out with GAUSSIAN94 default criteria. The 6-31G(d) polarization basis set was used for most calculations, because it is expected to give reasonably accurate structures, i.e. more in accord with experiment. Two other basis sets, 3-21G(d) and 6-311G(d,p), were also used for, respectively, HF/UHF and DF (and HF/DF) calculations. The detailed expressions for the Hartree–Fock [16], second-order Møller–Plesset perturbation (MP2) [17] and Kohn–Sham (KS) density functional [18] equations are well known and will not be reproduced here. An overview of the expressions for the molecular energies is, however, presented in order to facilitate the discussion of the results. The general expression for the KS molecular energy is [19]

$$E = V_{nn} + H^{core} + V_{ee} + E_x(\rho) + E_c(\rho) \qquad (2)$$

where the terms on the right represent, respectively, the nuclear–nuclear repulsion energy, the one-electron (kinetic and electron–nuclear interaction) energy, the Coulombic interaction energy (between electrons), the exchange energy and the correlation energy. The HF equations do not include correlation at all, and when E_x in Eq. 2 is given by the HF exchange, Eq. 2 (with $E_c = 0$) yields the HF molecular energy. The GAUSSIAN94 UMP2/MP2 models yield correlation energies, E_c, which are a function of the many-electron wave function and may be identified as analogous to $E_c(\rho)$. For cases where the spin contamination is large, the UMP2, spin-unrestricted DF and hybrid HF/DF calculations give, by default, the spin-annihilated UHF, UMP2, DF and hybrid HF/DF energies along with the expectation values ($\langle S^2 \rangle$) before and after spin annihilation (spin projection). The DF calculations in this work used three different combinations for the exchange-correlation functional: SVWN (Slater exchange (S) plus the correlation functional of Vosko, Wilk and Nusair (VWN) [13]); BLYP (Becke's exchange functional (B) [20] and the correlation functional of Lee, Yang and Parr (LYP) [21]); and B3LYP (hybrid HF exchange/DF exchange-correlation functional) [22]. The Becke exchange functional (B) includes the Slater exchange [23] along with corrections involving the gradient of the density [20]. The VWN functional includes only local correlation, while LYP includes both local (i.e. the VWN functional) and nonlocal (gradient-corrected) terms. The exchange-correlation functional of the semiempirical B3LYP model is Becke's three-parameter functional which has the form [19]:

$$AE_x^{Slater} + (1-A)E_x^{HF} + B\Delta E_x^{Becke} + CE_c^{LYP} + (1-C)E_c^{VWN} \qquad (3)$$

Results and Discussion

*Calculated structures for **I**, **VI** and **XI** and their radical anions*

The geometries of **I**, **VI** and **XI** calculated by only a few of the quantum chemical methods tested are presented here. The geometries of *p*-benzoquinone (**I**) calculated by a variety of methods had previously been com-

TABLE 4
COMPARISON OF BOND LENGTHS OF THE RADICAL ANIONS OF **I**, **VI** AND **XI** CALCULATED BY THE B3LYP/6-311G(d,p) AND AM1-HE METHODS

Bond	B3LYP/6-311G(d,p)			AM1-HE		
	I	**VI**	**XI**	**I**	**VI**	**XI**
C1-O	1.262	1.262		1.264	1.265	
C4-O	1.262			1.264		
C2-C3	1.369	1.373	1.371	1.361	1.363	1.361
C5-C6	1.364	1.369	1.371	1.361	1.360	1.361
C1-C2	1.452	1.450	1.445	1.450	1.446	1.452
C3-C4	1.452	1.442	1.442	1.450	1.451	1.451
C4-C5	1.452	1.442	1.445	1.450	1.453	1.452
C1-C6	1.452	1.453	1.442	1.450	1.448	1.451
C1-N			1.334			1.322
C4-N		1.335	1.334		1.323	1.322
N-H			1.025			0.999
N-H		1.026	1.025		0.999	0.999
C2-H	1.088	1.088	1.090	1.099	1.099	1.101
C3-H	1.088	1.091	1.087	1.099	1.101	1.101
C5-H	1.088	1.087	1.090	1.099	1.101	1.101
C6-H	1.088	1.088	1.087	1.099	1.099	1.101

Atom numbering as in Scheme 3.

TABLE 5
ELECTRONIC ENERGIES OF THE RADICAL ANIONS ($Q^{\bullet}$) OF **I**, **VI** AND **XI** AS CALCULATED BY VARIOUS MODELS

Model	Energy (au)		
	I	**VI**	**XI**
ROHF	–379.25097	–359.39473	–339.53476
UHF	–379.26246	–359.41088	–339.55093
PUHF	–379.27053	–359.42333	–339.56305
UMP2	–380.35847	–360.48076	–340.61929
PMP2	–380.36679	–360.49389	–340.63068
USVWN[a]	–379.57274	–359.75467	–339.93481
UBVWN[a]	–384.41485	–364.49137	–344.56615
UBLYP[a]	–381.51282	–361.60793	–341.70128
UB3LYP	–381.50992	–361.62050	–341.72917
UB3LYP[a]	–381.62005	–361.72529	–341.82852

[a] The basis set used was 6-311G(d,p); for all the others the 6-31G(d) basis set was used.

pared with experimental geometries of **I** by Boesch and Wheeler [24], who concluded that the second-order Møller–Plesset perturbation method (UMP2/6-31G(d)) and the local density functional method combining Slater's exchange functional with the correlation functional of Vosko, Wilk and Nusair [13] (SVWN/6-31G(d)) gave excellent bond distances and angles. The MP2 results for **I** in Table 1A are essentially identical to the results of Boesch and Wheeler [24], while the SVWN/6-311G(d,p) distances are only slightly shorter (by 0.001–0.005 Å) than the SVWN/6-31G(d) results of Boesch and Wheeler [24]. The AM1 results are in very good agreement with the MP2 distances, except for the C=C and C-H bond lengths which differ by 0.011 and 0.016 Å, respectively. This would indicate that the AM1 geometry for **I** is in good accord with experiment.

The bond distances in Table 1A lend themselves for the comparison of the geometries of **I**, **VI** and **XI**. All the methods indicate that the C=O bond distances in **I** and **VI** and the C=C bond distances in **I**, **VI** and **XI** are about the same, but perhaps with an increasing trend in the bond lengths in the order **I** < **VI** < **XI**. On the other hand, the MP2 and SVWN results clearly show a decreasing trend in going from **I** → **VI** → **XI**. By comparing the C=O, C=C and C-C bond distances in **I** with, respectively, the C=O double-bond distance in formaldehyde (1.203 Å), the C=C double-bond distance in ethylene (1.34 Å), the C-C single-bond distance in ethane (1.54 Å) and the 'aromatic' carbon–carbon distances in benzene (1.397 Å), Boesch and Wheeler [24] concluded that the C=O, C=C and C-C distances seem to indicate some conjugation between the C=O and C=C double bonds, but not complete electronic delocalization. Similar arguments can be made in the case of **VI** and **XI**. The slight increases in the calculated C=O and C=C double bonds and the slight decreases in the C-C single-bond distances in **VI** and **XI**, when compared to the respective bonds in **I**, may suggest that there is greater electronic delocalization in **VI** and **XI**. The calculated C=N double-bond distances of 1.3 Å in **VI** and **XI** are substantially shorter than the C-N single-bond distances of 1.43 Å in *N*-phenylacetamide [25] (which is expected to have some electron delocalization) and of 1.383 Å in pyrrole [25] (an aromatic cyclopentadiene [26]). On the other hand, the C=N bonds in **VI** and **XI** are not as long as the 'aromatic' carbon–nitrogen bond distance of 1.339 Å in pyridine [25] (a cyclic aromatic imine [26]) and not as short as the C=N double-bond distance of 1.273 Å in methyleneimine [27]. Thus, the electronic delocalization in **VI** and **XI** should be incomplete, suggesting that **VI** and **XI** may be described as bridges between aromatic and nonaromatic cyclic hydrocarbons, as is the case for **I**. The MP2 and SVWN bond angles shown in Table 1B vary by no more than 1°. The AM1 bond angles are also in good agreement with the MP2 and SVWN bond angles, except for the ∠CNH bond angles which differ from the MP2 and SVWN bond angles by 5–6°.

Since the B3LYP model appears to give the most accurate EA_{ad} data [28], some of the results obtained by this model are also presented here for further analysis of the geometry data. The B3LYP/6-31G(d) bond lengths and angles for **I**, **VI** and **XI** are also given in Table 1 (while a

TABLE 6
EXPECTATION VALUES OF THE RADICAL ANIONS BEFORE AND AFTER ($\langle S^2\rangle_a$) SPIN ANNIHILATION

	UHF[a]	UMP2[a]	USVWN[b]	UBVWN[b]	UBLYP[b]	UB3LYP[a]	UB3LYP[b]	AM1-UHF
I								
$\langle S^2\rangle$	0.853	0.866	0.751	0.752	0.753	0.762	0.762	0.81
$\langle S^2\rangle_a$	0.753	0.753	0.75	0.75	0.75	0.75	0.75	
VI								
$\langle S^2\rangle$	1.0	0.94	0.752	0.754	0.754	0.77	0.77	0.89
$\langle S^2\rangle_a$	0.8	0.77	0.75	0.75	0.75	0.75	0.75	
XI								
$\langle S^2\rangle$	0.91	0.92	0.752	0.754	0.76	0.77	0.77	0.95
$\langle S^2\rangle_a$	0.76	0.76	0.75	0.75	0.75	0.75	0.75	

[a] Basis set 6-31G(d).
[b] Basis set 6-311G(d,p).

TABLE 7
RATIOS OF SPIN DENSITIES CALCULATED BY VARIOUS QUANTUM CHEMICAL METHODS

Ratio	UHF[a]	UMP2[a]	USVWN[b]	UBVWN[b]	UBLYP[b]	UB3LYP[a]	UB3LYP[b]
I							
ρ_1/ρ_4	1.0	1.0	1.0	1.0	1.0	1.0	1.0
ρ_2/ρ_4	15.5	4.1	1.2	1.2	1.3	1.4	1.4
ρ_3/ρ_4	15.5	4.1	1.2	1.2	1.3	1.4	1.4
ρ_7/ρ_4	76.3	21.6	3.2	3.3	3.7	4.8	4.6
VI							
ρ_1/ρ_4	0.5	0.4	3.0	5.3	8.8	2.5	3.2
ρ_2/ρ_4	0.6	0.4	2.9	4.8	8.7	2.1	2.8
ρ_3/ρ_4	1.1	0.9	4.0	7.3	13.2	4.3	5.4
ρ_7/ρ_4	0.5	0.7	8.3	14.5	27.1	8.7	10.9
ρ_6/ρ_4	0.8	0.7	2.1	3.3	5.8	1.1	1.5
ρ_5/ρ_4	1.1	1.0	3.7	6.7	12.2	4.0	5.1
ρ_8/ρ_4	1.7	1.9	13.8	25.2	46.5	15.7	19.5
XI							
ρ_1/ρ_4	1.0	1.0	1.0	1.0	1.0	1.0	1.0
ρ_2/ρ_4	0.2	0.15	2.2	2.9	3.9	7.0	18.2
ρ_5/ρ_4	0.2	0.15	2.2	2.9	3.9	7.0	18.2
ρ_3/ρ_4	0.7	0.7	2.6	3.5	4.7	9.4	23.4
ρ_6/ρ_4	0.7	0.7	2.6	3.5	4.7	9.4	23.4
ρ_7/ρ_4	3.3	3.2	9.8	13.9	19.0	41.1	102.3
ρ_8/ρ_4	3.3	3.2	9.8	13.9	19.0	41.1	102.3

Atom numbering as in Scheme 3.
[a] Basis set 6-31G(d).
[b] Basis set 6-311G(d,p).

comparison of bond angles in the $Q^{\bullet-}$ forms of **I**, **VI** and **XI**, calculated by the B3LYP/6-31G(d) level, is presented in Table 2). These data can be compared to the rest of the data in Table 1 and the generally good agreement is apparent from the data. The B3LYP/6-311G(d,p) bond distances (not reported here) seemed to be slightly shorter than the B3LYP/6-31G(d) distances, but the differences between the two basis sets were no more than 0.007 Å (calculated for the C=O bond). Similarly, no significant differences were observed in the B3LYP bond angles calculated using the two basis sets. In order to assess the effect of electron attachment on the geometries of **I**, **VI** and **XI**, the calculated changes in geometry (bond lengths) upon electron attachment are presented in Table 2 for the B3LYP/6-31G(d) methods. Similarly calculated changes in bond lengths (Å) at the B3LYP/6-311G(d,p) level were essentially the same as those reported here. The positive and negative changes upon electron attachment in the skeletal double- and single-bond distances, respectively, are indicative of electron delocalization [29]. All the C-H and N-H bonds also get longer, but by a much lesser magnitude. From the lesser uniformity of the calculated changes in bond lengths for the semiquinone of **VI**, it might be inferred that the delocalization in the semiquinone of **VI** is to a lesser degree compared to that in **I** and **XI**.

A comparison of some selected bond lengths of the *p*-benzosemiquinone radicals of **I**, **VI** and **XI** with corresponding bond lengths in the phenoxyl radical, phenol and aniline can be made as shown in Table 3. In contrast to C-O and average C-C bond lengths (gas phase) in phenol, the B3LYP/6-31G(d) calculated C1-O and C2-C3 bond lengths are substantially shorter in $Q^{\bullet-}$ of **I**, while the C1-C2 bond length is longer than the C-C bond in phenol. This can be interpreted to mean that the electron delocalization in the radical anion of **I**, when compared to that in **I**, has not changed significantly to a more aromatic character. The same argument also holds for **VI** and **XI**. The C1-O bond length in $Q^{\bullet-}$ of **VI** (B3LYP/6-31G(d) calculated) is shorter than the C-O bond in phenol, while the C-N bond in $Q^{\bullet-}$ of both **VI** and **XI** and the C2-C3 bonds (in $Q^{\bullet-}$ of **VI** and **XI**)) are shorter than, respectively, the C-N and C-C bonds in aniline. On the other hand, the C1-C2 bonds (in $Q^{\bullet-}$ of **VI** and **XI**) are longer than the C-C bond in aniline. As will be discussed later, the radical anion of **I** is of the phenoxyl type and its geometry can also be compared to that of the phenoxyl radical. For example, the bond lengths of the bonds corresponding to C1-O, C2-C3 and C1-C2 (1.267, 1.372 and 1.453 Å (B3LYP/6-31G(d) calculated)) in $Q^{\bullet-}$ of **I** are 1.268, 1.386 and 1.467 Å (B3LYP/6-31G(d) calculated [30]) in the phenoxyl radical. This indicates that the C-O bond lengths in $Q^{\bullet-}$ of **I** and the phenoxyl radical are almost identical while the carbon–carbon bonds in $Q^{\bullet-}$ of **I** are shorter (by about 0.014–0.015 Å).

In order to make some assessment as to how comparable the geometries obtained by the AM1-HE and the

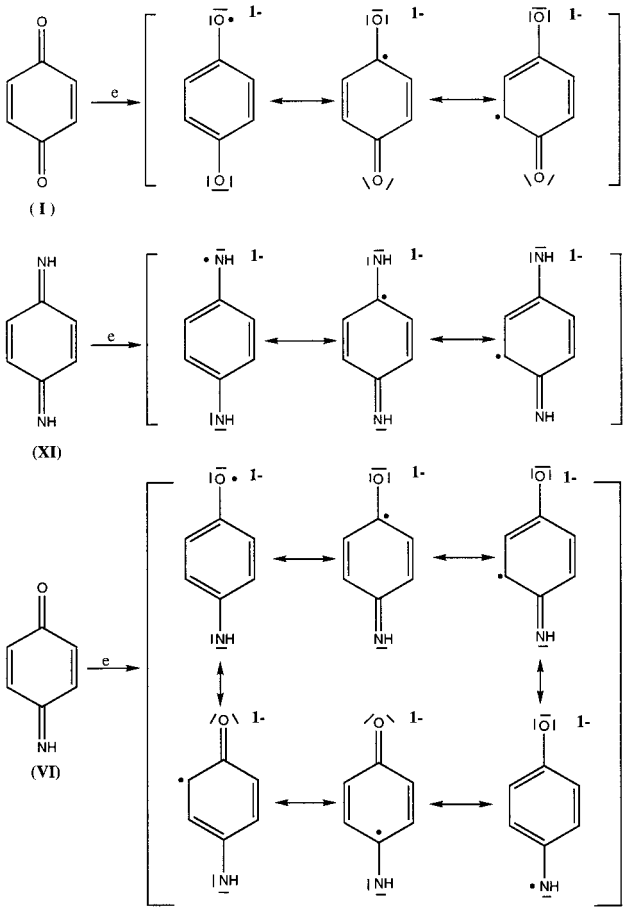

Scheme 2. Resonance/Lewis structures of the Q$^{\bullet-}$ forms of **I**, **VI** and **XI**.

B3LYP/6-311G(d,p) models are, the bond lengths of the radical anions obtained by these two methods are presented in Table 4. As can be judged by the data in Table 4, the AM1-HE bond lengths are in good accord with the B3LYP/6-311G(d,p) bond lengths, and the actual differences in the bond lengths are no more than 0.03 Å, with the variation being within about 0.01 Å in most cases.

*Electronic spin densities for the radicals of **I**, **VI** and **XI***

The computed electronic energies, expectation values ($\langle S^2 \rangle$) and ratios of spin densities are presented in Tables 5–7. A comparison of the expectation values before ($\langle S^2 \rangle$) and after ($\langle S^2 \rangle_a$) spin annihilation (Table 6) indicates the extent of spin contamination by higher spin states remaining after the first spin contaminant has been annihilated. While spin contamination is not significant in the USVWN, UBVWN and UBLYP ground states even prior to spin annihilation, the UHF and UMP2 ground-state wave functions contain some spin contamination even after spin annihilation. This, in turn, may affect the magnitude of the spin densities as well as the spin density ratios [31]. For the UHF and UMP2 cases, the degree of spin contamination before and after spin annihilation varies in the order **I** < **XI** < **VI**. The degree of spin contamination observed in the AM1-UHF ground-state wave functions seems to be comparable to, and may be slightly less than, that of the UHF and UMP2 wave functions. From work on the phenoxyl radical, Qin and Wheeler [30] have interpreted that density functional methods appear to lead to pure doublet states while the hybrid methods seem to present intermediate extents of spin contamination. This interpretation is consistent with the findings of Baker et al. [32], who showed that unrestricted Kohn–Sham wave functions are generally significantly less spin contaminated at equilibrium geometries than their unrestricted HF wave functions even for systems whose standard UHF wave functions exhibit major contamination. That spin annihilation improves the DFT wave function, and expectation values for observables other than the energy may also be calculated therefrom, has also been pointed out by Cramer et al. [33]. The results presented here are consistent with the above observations.

Upon examination of the calculated ratios of spin density data in Table 7, several inferences should be apparent. Some uniformity is observed in spin density ratios calculated by a given method for Q$^{\bullet-}$ of **I** and **XI**, but more so for Q$^{\bullet-}$ of **I**. In Q$^{\bullet-}$ of **XI**, the disposition of the H atoms introduces dissymmetry in the molecule and, thus, can lead to further localization of the unpaired electron compared to that in Q$^{\bullet-}$ of **I**. The localization of unpaired electrons is more prevalent in Q$^{\bullet-}$ of **VI**, as can be judged from the disparity of the spin density ratios. Overall, the data can be explained by the resonance/Lewis structures shown in Scheme 2. While the resonance structures indicate phenoxyl- and anilino(RNH)-type radicals, respectively, for **I** and **XI**, both phenoxyl- and anilino-type radical resonance structures contribute to the overall molecular structure in Q$^{\bullet-}$ of **VI**. Moreover, the anilino-type radical has the greatest spin density, i.e. on the N atom. A comparison of the spin density ratios among the different methods indicated that the magnitudes of the ratios decrease in the order UHF/UMP2 > DF > HF/DF for **I**, DF > HF/DF > UHF/UMP2 for **VI** and DF/HF > DF > UHF/UMP2 for **XI**.

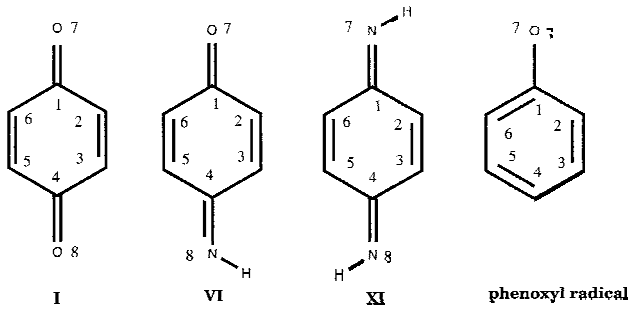

Scheme 3. Atom numbering for **I**, **VI**, **XI** and their radicals as well as the phenoxyl radical.

TABLE 8
ADIABATIC ELECTRON AFFINITIES (kcal/mol) CALCULATED BY VARIOUS QUANTUM CHEMICAL METHODS

Q	3-21G(d) UHF	6-31G(d)[a]		6-31G(d)						Expt[b]	Half-electron			AM1 (v)[c]	6-311G(d,p)			
		UHF	SVWN	ROHF	UHF	PUHF	UMP2	PMP2	B3LYP		SAM1	PM3	AM1		SVWN	BVWN	BLYP	B3LYP[d]
I	22.9	16.6	54.9	9.7	16.9	21.9	20.3	25.5	36.54	44.1[e]	37.2	47.8	48.7	40.0	58.51	59.68	38.65	42.58 (43.7)
VI	13.5	13.7	44.3	0.01	10.1	18.0	4.5	12.9	27.3	43.58[f]	32.7	42.6	40.7	31.6	48.41	50.3	29.26	33.07 (34.7)
XI	0.6	–1.8	35.3	6.2	3.9	11.5	0.1	6.8	18.17	44.04[g]	28.0	37.3	32.0	23.8	38.7	41.1	20.14	23.67 (25.8)

[a] Results are for single-point calculation on UHF/3-21G(d) geometry.
[b] Values (gas-phase electron free energies) are for **I** only.
[c] Vertical (Koopmans') EA.
[d] Values in parentheses are after correction for zero-point energy difference.
[e] Reference 12a.
[f] Reference 11.
[g] Reference 12b.

Except perhaps in the case of **I**, the variance in the calculated spin density ratios across the different methods is quite substantial. As to which method gives the more accurate spin density ratios cannot, thus, be determined in the absence of experimental data. However, the UHF and UMP2 wave functions, because they have greater spin contamination, may lead to more error in the spin density ratios [31]. In the case of $Q^{\bullet-}$ of **I**, for which experimental data are available [34], the magnitudes of the spin densities (ρ) at positions 2, 3, 5 and 6 are equal. From the data in Table 7, it is seen that $\rho_2/\rho_4 = \rho_3/\rho_4$ (and, also, $\rho_5/\rho_4 = \rho_6/\rho_4 = \rho_2/\rho_4$), indicating that $\rho_2 = \rho_3 = \rho_5 = \rho_6$. Not only is this consistent with the experimental observation [34], but it is also reproduced by all the methods tested. It might also be interesting to compare the spin density ratios for $Q^{\bullet-}$ of **I** with those for the phenoxyl radical [30,34,35]. The experimentally derived spin density ratios for the phenoxyl radical [34,35] are $\rho_2/\rho_4 = 0.7$ and $\rho_3/\rho_4 = 0.18$ (numbering as in Scheme 3). The corresponding values, as calculated by the various methods (Table 7), for the *p*-benzosemiquinone radical anion of **I** are substantially higher, indicating that the spin density at position 4 in $Q^{\bullet-}$ of **I** is more depleted. This can be explained by the presence of the second electronegative O atom in **I**. The ρ_7/ρ_4 ratios calculated for the phenoxyl radical were 0.83 (UHF), 0.56 (UMP2) and 0.88–1.2 (DF and hybrid HF/DF) [30]. For $Q^{\bullet-}$ of **I**, the ρ_7/ρ_4 ($=\rho_8/\rho_4$) ratios are all higher, with the UHF and UMP2 results being a lot more so. This seems to suggest that the presence of the second O atom leads to more depletion of the spin density at positions 4 (and 1). For the phenoxyl radical, the SVWN density functional approximation has been reported to give the most accurate spin density ratios [30]. Whether the same is true for $Q^{\bullet-}$ of **I** cannot be ascertained in this work. Except for the UHF and UMP2 results, the ratios obtained by the DF and hybrid HF/DF methods seem to agree with each other for $Q^{\bullet-}$ of **I**. This is not, however, the case for $Q^{\bullet-}$ of **VI** and **XI**. Nevertheless, despite the significant variance in the calculated ratios among the different methods, the relative ratios for a given method appear to agree, on average, with the other methods. This would suggest that the relative spin density distribution by any of the methods should provide a reasonable overall representation of the spin density distribution for the radicals.

Adiabatic electron affinities (EA_{ad}'s)

The adiabatic electron affinities of **I**, **VI**, and **XI** calculated by the various methods are presented in Table 8. The calculated values for **I** can be compared with that experimentally derived (42–44 kcal/mol) [11,12] to gauge the performance of the different methods. The first set includes UHF/3-21G(d), UHF/6-31G(d)//UHF/3-21G(d) and SVWN/6-31G(d)//UHF/3-21G(d) calculated EA_{ad}'s. Clearly, the UHF results are very low. The SVWN results are significantly higher, but the method overestimates the EA_{ad} of **I** by about 12 kcal/mol. The PUHF/6-31G(d) and PMP2/6-31G(d) results are modestly better than the UHF and UMP2 results, but not much better than the UHF/3-

TABLE 9
CALCULATED DIFFERENCES IN ADIABATIC ELECTRON AFFINITY AT VARIOUS LEVELS OF THEORY

Method	Difference (kcal/mol)	
	EA_{ad}(**I**) – EA_{ad}(**VI**)	EA_{ad}(**VI**) – EA_{ad}(**XI**)
UHF[a]	9.4	12.9
PUHF[b]	4.0	6.4
UMP2[b]	15.9	4.3
PMP2[b]	12.7	6.0
SAM1-HE	4.5	4.7
PM3-HE	5.2	5.3
AM1-HE	8.0	8.7
AM1 (Koopmans')	8.4	7.9
SVWN[c]	10.1	9.7
BVWN[c]	9.4	9.2
BLYP[c]	9.4	9.1
B3LYP[b]	9.2	9.1
B3LYP[c]	9.5	9.4

[a] Basis set 3-21G(d).
[b] Basis set 6-31G(d).
[c] Basis set 6-311G(d,p).

TABLE 10
LUMO ORBITAL ENERGIES (eV) FOR **I**, **VI** AND **XI** CALCULATED BY A VARIETY OF QUANTUM CHEMICAL METHODS

Q	AM1	RHF[a]	MP2[a]	SVWN[b]	BVWN[b]	BLYP[b]	B3LYP[a]	B3LYP[b]
I	–1.735	0.598	0.09	–5.243	–5.223	–4.306	–3.538	–3.734
VI	–1.372	0.996	0.573	–4.732	–4.737	–3.821	–3.061	–3.256
XI	–1.031	1.443	1.038	–4.24	–4.272	–3.356	–2.601	–2.791

[a] Basis set 6-31G(d).
[b] Basis set 6-311G(d,p).

21G(d) results, despite the use of a larger basis set and the inclusion of spin annihilation in the calculation [36]. The ROHF result is apparently the poorest in at least two ways: the method calculates the lowest EA_{ad} for **I**, and yields an EA_{ad} for **VI** that is lower than the EA_{ad} for **XI**. Although the ROHF model has no spin contamination problem for open shell systems (because it uses the same set of spatial orbitals for the α and β spin orbitals, and the wave function is an eigenfunction of $\hat{S}^2$) [37], not surprisingly it raises the energy of the radical anion and underestimates EA_{ad}. The UHF wave functions are not eigenfunctions of $\hat{S}^2$, and suffer from spin contamination when this is large [31]. Spin contamination in the UHF wave function is not reduced significantly [31] or at all, as the data in Table 8 show, by perturbation correction for electron correlation and the EA_{ad} calculated is poor. Spin-projected UHF (PUHF) and approximate spin-projected UMP2 (PMP2) methods [36] perform a little better, but still the EA_{ad}'s calculated are too low. As the data in Table 8 show, modest improvements are made by all the semiempirical methods. The SVWN and BVWN DF methods overestimate the EA_{ad} of **I** at the level of the 6-311G(d,p) basis set. On the other hand, both BLYP/6-311G(d) and B3LYP/6-31G(d) underestimate the EA_{ad} of **I**. The B3LYP/6-311G(d,p) EA_{ad} is, however, in excellent agreement with the experimentally derived EA_{ad} of **I**. In all the cases, except for the ROHF method, the EA_{ad}'s of **I**, **VI** and **XI** vary in the order **I** > **VI** > **XI**. It is also apparent from the data that the DF, hybrid HF/DF and the AM1-HE methods predict the same trend for the EA_{ad}'s of **I**, **VI** and **XI**, with the difference in the EA_{ad}'s of **I** and **VI**, and the EA_{ad}'s of **VI** and **XI**, being 8–10 kcal/mol (Table 9).

The calculated trend in EA_{ad} can be rationalized by a consideration of the calculated LUMO orbital energies of **I**, **VI** and **XI**. The LUMO orbital energies in Table 10 for **I**, **VI** and **XI** vary in the order **I** < **VI** < **XI**. In the electron attachment process, the extra electron enters the LUMO orbital, and the lower the LUMO energy, the higher the electron affinity [12]. The substitution of =O by =NH in **VI** and **XI** raises the energy of the LUMO and, hence, lowers the electron affinity. The EA_{ad} values are, thus, in agreement (except for the ROHF method) with the predicted electron affinity trend based on the LUMO energies. The reason for the lowering of the electron affinity can be rationalized further by a consideration of selected atomic charges for the Q and $Q^{\bar{\bullet}}$ forms and spin densities for the $Q^{\bar{\bullet}}$'s. The Mulliken atomic charges at the B3LYP/6-311G(d,p) level for Q and $Q^{\bar{\bullet}}$ of **I**, shown in Scheme 4, are uniformly dispersed. Such is not, however, the case for the Q and $Q^{\bar{\bullet}}$ forms of **VI** and **XI**, in which the distribution of the charges is not as uniform, more so in the case of **VI**. This can be realized better when the charge on the H atom is summed with the charge on the N atom. A consideration of the spin density distribution (Scheme 4) in the radical anions leads to the same conclusion as that for the atomic charges.

The UB3LYP spin densities of the heavy atoms of $Q^{\bar{\bullet}}$ of **I** are shown (Scheme 4) to be less than 0.1 (and for the

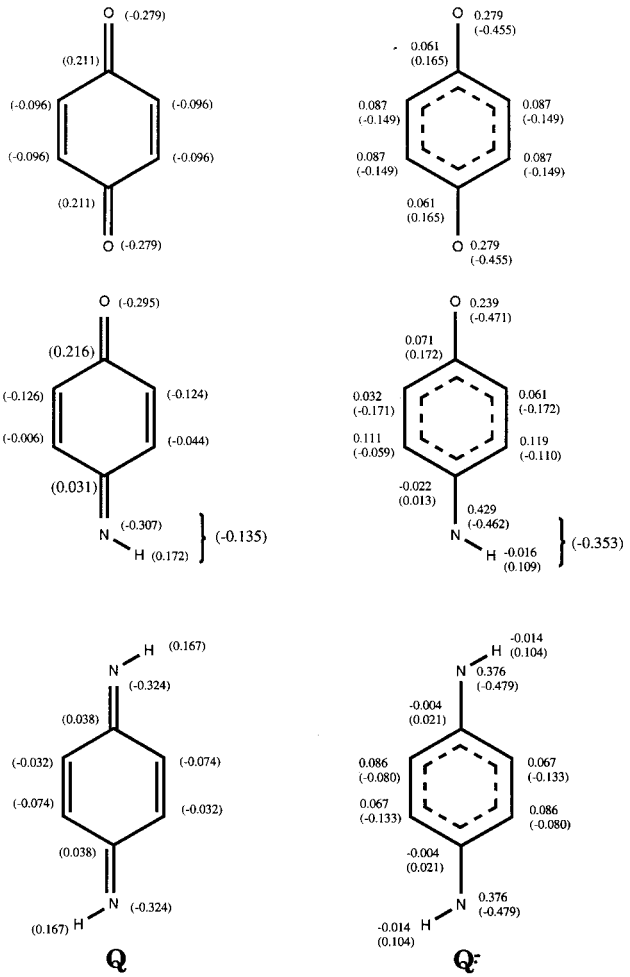

Scheme 4. Mulliken charges (in parentheses) and spin densities (for the $Q^{\bar{\bullet}}$ forms) as calculated by the B3LYP/6-311G(d,p) method.

H atoms as well; not shown) except for the O atoms, the spin densities of which are about 0.28. The spin densities of the heavy atoms in the case of $Q^{\bullet}$ of **VI** and **XI** are, however, substantially different in magnitude (differences are observed in sign as well), and the highest spin density is on the N atom (0.43 and 0.38 in the $Q^{\bullet}$ forms of **VI** and **XI**, respectively). We had recently compared the reactivities of the redox states of **I** and **VI** by using electrostatic potentials (V(r)) [7]. From calculated maximum electrostatic potentials (V_{max}), the electrophilic site in **VI** is due to the N-H group and the greater spin density at the N atom might be explained by the electrophilicity of the N-H region localizing the unpaired electron at this region.

It is of interest to make two other observations with regard to the data in Tables 8 and 10. First, the data in Table 8 allow the assessment, though limited, of gradient correction on the exchange and correlation functionals of the density functional models used, and the effect of basis set on the quality of the calculated adiabatic electron affinities. At the VWN level, no improvement was gained from the use of the Becke gradient correction to the Slater exchange functional; if anything, the data get poorer. However, gradient correction to the correlation functional leads to substantial improvement. Still further improvement is obtained from the use of the hybrid HF/DF method. The use of the 6-31G(d) basis set lowers the electron affinity by 0.24–0.26 eV, indicating that the 6-311G(d,p) basis set is more appropriate. Overall, correction for the nonuniformity of the electron density is apparently much more important. Second, the LUMO energies in Table 10 provide the correct trend, with the AM1 LUMO energies actually being in reasonable accord with the UB3LYP calculated EA_{ad}'s. In fact, the AM1 vertical (Koopmans' [38]) electron affinities (40, 31.6 and 23.8 kcal/mol for **I**, **VI** and **XI**, respectively) are more in line with the UB3LYP calculated adiabatic electron affinities than the adiabatic electron affinities calculated by the AM1-HE method are.

Conclusions

The EA_{ad}'s calculated by most of the methods explored varied in the order **I** > **VI** > **XI** and this trend can be adequately rationalized by a consideration of LUMO orbital energies (of **I**, **VI** and **XI**), Mulliken atomic charges of the neutral molecules and their radical anions, and spin density distributions in the radical anions. The differences in the calculated electron affinities, EA_{ad}(**I**) – EA_{ad}(**VI**) and EA_{ad}(**VI**) – EA_{ad}(**XI**), were consistently found to be 8–10 kcal/mol in the case of the AM1, DF(SVWN, BVWN and BLYP) and hybrid HF/DF(B3LYP) models. This constancy in the electron affinity difference, coupled with the good accuracy of the calculated EA_{ad} of **I** by the B3LYP/6-311G(d,p) method, leads to the prediction of a quantitative trend in EA_{ad} of 42.6 > 33.1 > 23.7 corresponding to the trend EA_{ad}(**I**) > EA_{ad}(**VI**) > EA_{ad}(**XI**). The general utility of the B3LYP/6-311G(d,p) level of theory for the accurate prediction of trends in adiabatic electron affinities will be explored further in future work. Interestingly, the AM1 vertical (Koopmans') electron affinities are in good accord, though it may be fortuitous, with the B3LYP/6-311G(d,p) results.

Conventional analysis of the calculated structural data for **I** and **VI** (and **XI**) did not reveal any distinct structural difference between **I** and **VI** upon electron attachment. However, analysis of the spin density data predicted that phenoxyl- and anilino-type radical anions predominate in the *p*-benzosemiquinones of **I** and **XI**, respectively, while both phenoxyl- and anilino-type radical anions contribute to the average calculated structure of the *p*-benzosemiquinone of **VI**, with the contribution of the anilino type predominating. This difference, in addition to the difference in electron affinity, may play a significant role in the biochemical activity of the anthracyclines. Even though **I** and **VI**, as model systems for the anthracyclines, grossly oversimplify the structure of the pharmacophore of the anthracyclines, the results of this study give some insight and clues towards the understanding of the redox chemistry of structurally modified anthracyclines, and can also serve as a basis for future similar work.

Acknowledgements

This work was supported by the HHS/MBRS Program, Grant No. S06-GM08247. This work has also benefited from the financial support for computer and software maintenance by a grant from NSF/MRCE (Grant No. HRD-915407) and partial support by a Research Centers in Minority Institutions award, G12RR03062, from the Division of Research Resources, National Institute of Health. We acknowledge the comments of a reviewer who drew our attention to Ref. 33.

References

1 Acton, E.M., In Priebe, W. (Ed.) Anthracycline Antibiotics, ACS Symposium Series Vol. 574, American Chemical Society, Washington, DC, U.S.A., 1995, pp. 1–13.

2 Myers, C.E., Muinda, J.R.F., Zweier, J. and Sinha, B.K., J. Biol. Chem., 262 (1987) 11571, and references cited therein.

3 a. Lown, J.W., Chen, H.H. and Plambeck, J.A., Biochem. Pharmacol., 28 (1979) 2563.

b. Lown, J.W., Chen, H.H. and Plambeck, J.A., Biochem. Pharmacol., 31 (1982) 575.

c. Vavies, K.J.A., Doroshow, J.H. and Hochstein, H.P., FEBS Lett., 153 (1983) 227.

d. Mimnaugh, E.G., Trush, M.A., Ciarrocchi, E.G., Lestingi, M., Fontana, M., Spadasi, S. and Montecucco, A., Biochem. J., 279 (1991) 141.

e. Nafzinger, J., Auclair, C., Florent, J.C., Guillosson, J.J. and Monneret, C., Lechemie Res., 15 (1991) 709.
f. Mimnaugh, E.G., Trush, M.A., Ginsburg, E. and Gram, T.E., Cancer Res., 42 (1982) 3574.
4 Abdella, B.R.J. and Fisher, J., J. Environ. Health Perspect., 64 (1985) 3.
5 a. Davies, K.J.A. and Doroshow, J.H., J. Biol. Chem., 261 (1986) 3060.
b. Davies, K.J.A. and Doroshow, J.H., J. Biol. Chem., 261 (1986) 3068.
6 a. Favandon, K., Biochemie, 64 (1982) 457.
b. Lown, J.W., Acc. Chem. Res., 15 (1982) 381.
c. Dodd, N.J.F. and Mucherjee, T., Biochem. Pharmacol., 33 (1984) 379.
d. Nohland, H. and Jordan, W., Biochem. Biophys. Res. Commun., 114 (1983) 197.
7 Mariam, Y.H. and Sawyer, A., J. Comput.-Aided Mol. Design, 10 (1996) 441.
8 Ziegler, T. and Gutsev, G.L., J. Comput. Chem., 13 (1992) 70.
9 Dewar, M.J.S., Hashmall, J.A. and Venier, C.G., J. Am. Chem. Soc., 90 (1968) 1953.
10 Dewar, M.J.S. and Rzepa, H.S., J. Am. Chem. Soc., 100 (1978) 784.
11 Cooper, C.D., Naft, W.T. and Compton, R.N., J. Chem. Phys., 63 (1975) 2752.
12 a. Heinis, T., Chowdhury, S., Scott, S.L. and Kebarle, P., J. Am. Chem. Soc., 110 (1988) 400.
b. Chowdhury, S., Grimsrud, E.P. and Kebarle, P., J. Phys. Chem., 90 (1986) 2747.
13 Vosko, S.H., Wilk, L. and Nusair, M., Can. J. Phys., 58 (1980) 1200.
14 SPARTAN User's Guide, v. 4.0, Wavefunction, Irvine, CA, U.S.A., 1995.
15 Frisch, M.J., Trucks, G.W., Schlegel, H.B., Gill, P.M.W., Johnson, B.G., Robb, M.A., Cheeseman, J.R., Keith, T., Petersson, G.A., Montgomery, J.A., Raghavachari, K., Al-Laham, M.A., Zakrzewski, V.G., Ortiz, J.V., Foresman, J.B., Cioslowski, J., Stefanov, B.B., Nanayakkara, A., Challacombe, M., Peng, C.Y., Ayala, P.Y., Chen, W., Wong, M.W., Andres, J.L., Replogle, E.S., Gomperts, R., Martin, R.L., Fox, D.J., Binkley, J.S., Defrees, D.J., Baker, J., Stewart, J.P., Head-Gordon, M., Gonzalez, C. and Pople, J.A., GAUSSIAN, 94, Revision D.1, Gaussian Inc., Pittsburgh, PA, U.S.A., 1995.
16 a. Hehre, W.J., Radom, L., Schleyer, P.v.R. and Pople, J.A., Ab Initio Molecular Orbital Theory, Wiley, New York, NY, U.S.A., 1986.
b. Levine, I.N., Quantum Chemistry, Prentice-Hall, Englewood Cliffs, NJ, U.S.A., 1993.
17 a. Møller, C. and Plesset, M.S., Phys. Rev., 46 (1934) 618.
b. Pople, J.A., Binkley, J.S. and Seeger, R., Int. J. Quantum Chem. Quantum Chem. Symp., 10 (1976) 1.
18 a. Kohn, W. and Sham, L.J., Phys. Rev., A140 (1965) A1133.
b. Pople, J.A., Gill, P.M.W. and Johnson, B.G., Chem. Phys. Lett., 199 (1992) 557.
19 GAUSSIAN94 User's Reference, Gaussian Inc., Pittsburgh, PA, U.S.A., 1994–1995.
20 Becke, A.D., Phys. Rev., A38 (1988) 3098.
21 Lee, C., Yang, W. and Parr, R.G., Phys. Rev., B37 (1988) 785.
22 Becke, A.D., J. Chem. Phys., 98 (1993) 5648.
23 Slater, J.C., Quantum Theory of Molecules and Solids, Vol. 4, McGraw-Hill, New York, NY, U.S.A., 1974.
24 Boesch, S.E. and Wheeler, R.A., J. Phys. Chem., 99 (1995) 8125.
25 Gordon, A.R. and Ford, R.A., The Chemist's Companion, Wiley, New York, NY, U.S.A., 1972, pp. 105–108.
26 Vollhardt, K.P.C., Organic Chemistry, Freeman, New York, NY, U.S.A., 1987, pp. 1189–1198.
27 Hehre, W.J., Radom, L., Schleyer, P.v.R. and Pople, J.A., Ab Initio Molecular Orbital Theory, Wiley, New York, NY, U.S.A., 1986, pp. 165–173.
28 Wheeler, R.A., J. Am. Chem. Soc., 116 (1994) 11048.
29 Robinson, H.H. and Kahn, S.D., J. Am. Chem. Soc., 112 (1990) 4728.
30 Qin, Y. and Wheeler, R.A., J. Chem. Phys., 102 (1995) 1687.
31 Schlegel, H.B., J. Chem. Phys., 84 (1986) 4530.
32 Baker, J., Scheiner, A. and Andzelm, J., Chem. Phys. Lett., 216 (1993) 380.
33 Cramer, C.J., Dulles, F.J., Giesen, D.J. and Almlof, J., Chem. Phys. Lett., 245 (1995) 165.
34 a. Neat, P. and Fessenden, R.W., J. Phys. Chem., 78 (1974) 523.
b. West, P.R., Harman, L.S., Josephy, P.D. and Mason, R.P., Biochem. Pharmacol., 33 (1984) 2933.
35 Stone, T.J. and Waters, W.A., Proc. Chem. Soc., (1962) 253.
36 Schlegel, H.B., J. Chem. Phys., 92 (1988) 3075.
37 Chen, W. and Schlegel, H.B., J. Chem. Phys., 101 (1994) 5957.
38 Koopmans, T., Physica, 1 (1934) 104.
39 Lide, D.R. (Ed.), CRC Handbook of Chemistry and Physics, 76th ed., CRC Press, Boca Raton, FL, U.S.A., 1995–1996.